

Path Integral Particle Filtering for Hybrid Systems via Saltation Matrices

Karthik Shaji ^{*}, Sreeranj Jayadevan [†], Bo Yuan [‡], Hongzhe Yu [§], Yongxin Chen [¶]
Georgia Institute of Technology, Atlanta, GA, 30332

We present an optimal-control-based particle filtering method for state estimation in hybrid systems that undergo intermittent contact with their environments. We follow the path integral filtering framework that exploits the duality between the smoothing problem and optimal control. We leverage saltation matrices to map out the uncertainty propagation during contact events for hybrid systems. The resulting path integral optimal control problem allows for a state estimation algorithm robust to outlier effects, flexible to non-Gaussian noise distributions, that also handles the challenging contact dynamics in hybrid systems. This work offers a computationally efficient and reliable estimation algorithm for hybrid systems with stochastic dynamics. We also present extensive experimental results demonstrating that our approach consistently outperforms strong baselines across multiple settings.

I. Introduction

The objective of filtering in dynamic systems is to estimate the “true” state of a given system in the presence of sensor measurements. In continuous-time Aerospace systems, three commonly used paradigms are the Kalman filter (KF) [1], the Extended Kalman filter (EKF) [2], as well as the Unscented Kalman filter (UKF) [3, 4]. One common downside to all of these algorithms is that they intrinsically assume the noise distribution is close to Gaussian, and their performance degrades under non-Gaussian noise [5, 6]. For systems that exhibit colliding contact with their environment, such as legged locomotion [7], robotic grasping and manipulation [8], and impact-driven mechanical systems [9], this difficulty is only further amplified. These hybrid systems transition between modes based on contact events, making state estimation particularly challenging due to sudden, discontinuous changes in dynamics. This area of work has shown increasing value, with application to extraplanetary robotics, such as the super-ball bot and tensegrity robotics projects [10, 11], trajectory optimization for planetary landing schemes (which make contact on landing) [12], and Rendezvous, Proximity Operations and Docking (RPOD) [13].

One method to get around challenges with non-Gaussian noise distributions is through particle filtering [14], also

^{*}Graduate Student, Daniel Guggenheim School of Aerospace Engineering

[†]MathWorks

[‡]Graduate Student, Daniel Guggenheim School of Aerospace Engineering

[§]PlusAI

[¶]Associate Professor, Daniel Guggenheim School of Aerospace Engineering

known as Monte Carlo filtering, where a given state is estimated by an ensemble of particles, with their own weight. One commonly used approach is the Sequential Importance Resampling (SIR) filter, where the particle weight update is performed through approximating inter-particle relative posterior probabilities [15]. It is known that as the number of particles increases, the state estimate more closely resembles the posterior distribution of the noise [16]. One major problem with particle filters is the so-called “weight degeneracy problem,” where individual particles can possess a high relative weight compared to the rest, and the estimation characteristics end up degrading [17]. One way around weight degeneracy is through increasing particle counts, either in a fixed or adaptive manner [18], as it increases the time it takes for weight degeneracy to occur, but that leads to higher computation times [19]. Sequential Importance Resampling aims to get around this issue by periodically resampling the particle weights and states once a resampling threshold is reached, but this operation does not scale well to high-dimensional problems, where higher-order state dimensions and greater particle counts are needed [20].

To address challenges with weight degeneracy, we follow the path integral particle filtering framework and leverage the duality between estimation and optimal control for continuous-time systems [21]. A useful lens for understanding nonlinear smoothing is its duality with stochastic optimal control: rather than treating inference purely as Bayesian filtering, state estimation can be posed as an optimal control / variational problem over state trajectories [22]. Optimal feedback laws and their associated posterior path distributions can be approximated using Monte-Carlo sampling, connecting smoothing/inference with sampling-based control computation.

Using this duality, we compute a posterior estimate by computing a suboptimal solution to an optimal control problem, developing a particle filter with better performance. The particular advantage of our work is the consideration of the time history of state evolution [23], whereas most commonly used particle filtering approaches only use the present sampling [15]. The major advantage of this approach is that it enables the correction of previous outliers and allows the algorithm to mitigate particle degeneracy and reduce the occurrence of expensive resampling steps.

We build on [24], which proposed a path integral particle filtering formulation for continuous-time systems. We extend this prior work to hybrid systems, characterized by continuous and discrete actions [25], in contact-driven domains. Traditional classical control and estimation methods struggle with this due to their underlying smooth and continuous assumptions [26]. With state estimation, one has to not only consider the present mode but also avoid potential combinatorial problems from multiple mode mismatches [27] between nominal and estimated dynamics in propagation calculations. In contrast to systems described solely by linear or nonlinear continuous-time dynamics, hybrid systems include discrete modes that must be specified alongside the continuous equations to fully characterize the system. Hybrid systems are represented using hybrid automata [28], with each mode defined by its own dynamics, as shown in Fig. 1. Mode transitions are triggered by guard conditions, may apply reset maps, and, for linear systems, involve switching between different sets of system matrices. For nonlinear systems, this involves changing the stochastic differential equations associated with each mode [29].

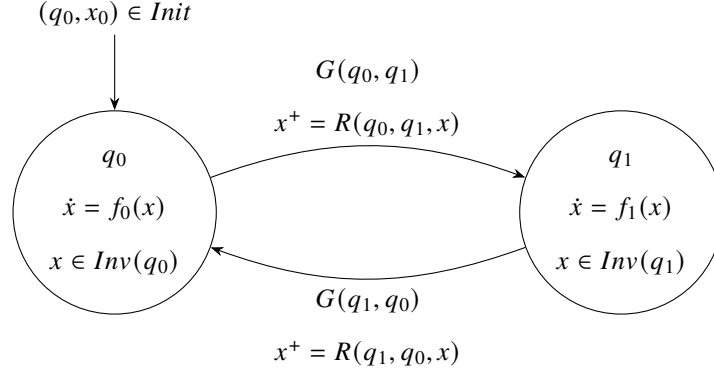


Fig. 1 Hybrid automaton with two modes

Existing estimation methods, including the previous continuous-time path integral particle filter [24], depend on understanding how probability distributions or uncertainties evolve through system dynamics [30]. This task becomes significantly more complicated in hybrid systems, where mode transitions may change the dimensionality of the state or modify the measurable states [31]. State estimation for such systems has been difficult, with novel methods being employed for many scenarios [32, 33]. [34] presents the Multiple Model Adaptive Estimation (MMAE) method, in which Kalman filters operate in parallel with a mode-probability mixing mechanism. A hybrid model of an aircraft with multiple modes that represent the flight regimes was used to accurately represent the dynamics of an aircraft. The paper models the dynamical system as a discrete-time stochastic linear hybrid system. While MMAE shows promising performance, it shares the same fundamental limitation as the previously discussed approaches: it is restricted to linear system models with Gaussian noise. More recently [35] has also leveraged the concept of saltation matrix, a tool for analysis of non-smooth systems, in the context of Kalman-like Filters, developing the Salted Kalman Filter (SKF) [36]. One key advantage of using the saltation matrix is that it gives a first-order approximation of the uncertainty propagation and dynamics changes from hybrid transitions, purely by using the Jacobian of the reset map [37]. By pairing that with a new dynamics model for the new mode, one can properly estimate a Gaussian noise distribution about a contact event. For the optimal control problem, we use the framework developed in [38] for a salted iLQR algorithm, but change the cost function in the continuous-time domain to meet the needs of our algorithm. We also employ the path integral control for hybrid systems as a basis for our method, from [39]. Our goal is to provide an algorithm that can perform accurate state estimation for hybrid dynamical systems, even when the noise follows non-Gaussian distributions, addressing a drawback in the method presented by [37]. [37] also briefly touches upon the topic of using Particle Filters for state estimation for hybrid systems. They avoided particle filters because of their computational cost, a concern that [40] later improved upon. In hybrid systems, the state dimension may change across modes, making state estimation especially challenging at transition points. Hence, as mentioned before, we follow the reference-trajectory extension

approach introduced in [36, 39], which provides a consistent way to extend trajectories across modes and improves estimation accuracy.

The results from our algorithm, the Salted Path Integral Particle Filter (SPIPF) are more accurate and computationally efficient compared to a traditional particle filter algorithm such as a multi-mode version of the SIR filter [15]. We compare the results against the baselines and the true posterior results. We test this on two different hybrid systems: the bouncing ball system and the Spring Loaded Inverted Pendulum (SLIP) system. The first system has linear dynamics, whereas the SLIP system has nonlinear dynamics [36]. The primary goal of our paper is to demonstrate improved contact estimation compared to other particle filter baselines on Gaussian noise distributions, whilst relying on the distribution-agnosticity of particle filters to generalize performance under non-Gaussian noise. Thus, the contributions of this paper are twofold.

Our paper is organized as follows: Section II discusses the mathematics and relevant notations, Section III discusses our new problem formulation, Section IV discusses the algorithm and its implementation, Section V explains the experiments used to validate performance, Section VI provides results compared to relevant baselines, and Section VII provides our conclusion and areas of future work.

II. Notation and Preliminaries

A. Smooth Path Integral Particle Filtering

The goal of this section of the paper is to discuss how a smooth filtering problem can be converted into an analogous optimal control problem. The authors in [24] used this duality to illustrate how controlled processes can be used to convert a posterior estimation problem into an optimal control one. We start with the following set of stochastic dynamics, where X_t is the nominal stochastic model, and Y_t is the measurement. The state dynamics X_t has a stochasticity described with the Wiener process $W_t \in \mathbb{R}^p$. The measurement $Y_t \in \mathbb{R}^p$ is corrupted by the standard Wiener process $B_t \in \mathbb{R}^p$ weighted by $\sigma_B > 0$ and the initial state X_0 follows the prior distribution ν_0 . We denote $h(t, X_t)$ by h_t for brevity, and the two Wiener processes W_t and B_t are defined as independent. The goal of the smoothing problem is a sequential filtering problem where the goal is to find the posterior distribution of X_t given the history of Y_t for $0 \leq t \leq T$, parameterized by the following,

$$dX_t = b(t, X_t)dt + \sigma(t, X_t)\sqrt{\epsilon}dW_t, \quad X_0 \sim \nu_0 \quad (1a)$$

$$dY_t = h(t, X_t)dt + \sigma_B dB_t, \quad Y_0 = 0. \quad (1b)$$

The authors in [21] found that this type of problem could be reformulated as a stochastic optimal control problem. Let us denote the measure over the path space Ω for the nominal dynamics in Eq. (1a) induced by \mathcal{P} , serving as the prior for

a Bayesian inference problem, while the posterior distribution is denoted by Q^Y . By the pathwise Kallianpur-Striebel formula [41], the ratio between Q^Y and \mathcal{P} enjoys an explicit form as

$$\frac{dQ^Y}{d\mathcal{P}} \propto \exp \left\{ -\frac{1}{\sigma_B^2} \left[\int_0^T Y_t dh_t + \frac{1}{2} \|h_t\|^2 dt - Y_T h(T, X_T) \right] \right\}. \quad (2)$$

From Equation (2), we can see the right-hand side as the likelihood of the observation process given the signal path. Let us denote the path distribution of the controlled process

$$d\tilde{X}_t = b(t, \tilde{X}_t) dt + \sigma(t, \tilde{X}_t)(u_t dt + \sqrt{\epsilon} dW_t), \quad \tilde{X}_0 \sim \pi_0 \quad (3)$$

as $\tilde{\mathcal{P}}$. As was derived in [42], we can now rewrite Equation (2) as the variational form of a smoothing problem aiming to find the distribution $\tilde{\mathcal{P}}$ that minimizes the following variational equation

$$\mathbb{E}_{\tilde{\mathcal{P}}} \left(\log \frac{d\tilde{\mathcal{P}}}{dQ^Y} \right) = \mathbb{E}_{\tilde{\mathcal{P}}} \left(\log \frac{d\tilde{\mathcal{P}}}{d\mathcal{P}} - \log \frac{dQ^Y}{d\mathcal{P}} \right) = \text{KL}(\tilde{\mathcal{P}} \parallel \mathcal{P}) - \mathbb{E}_{\tilde{\mathcal{P}}} \left(\log \frac{dQ^Y}{d\mathcal{P}} \right), \quad (4)$$

where the KL divergence is defined between the path space of the controlled and uncontrolled probability distributions $\tilde{\mathcal{P}}$ and \mathcal{P}

$$\text{KL}(\tilde{\mathcal{P}} \parallel \mathcal{P}) = \int d\tilde{\mathcal{P}} \log \frac{d\tilde{\mathcal{P}}}{d\mathcal{P}}. \quad (5)$$

We can now apply Girsanov theorem [43], but to the filtering problem, with the key difference that Equation (3) does not follow the same distribution as Equation (1a), from which we arrive at

$$\text{KL}(\tilde{\mathcal{P}} \parallel \mathcal{P}) = \mathbb{E} \left(\int_0^T \frac{1}{2\epsilon} \|u_t\|^2 dt \right) + \text{KL}(\pi_0 \parallel \nu_0). \quad (6)$$

We now plug in Equation (2) and Equation (6) into Equation (4), arriving at our optimal control formulation [21],

$$\min_{u, \pi_0} \mathbb{E} \left(\int_0^T l(t, X_t, u_t) + \Psi_T(X_T) \right) + \text{KL}(\pi_0 \parallel \nu_0), \quad (7)$$

where the extra term $\text{KL}(\pi_0 \parallel \nu_0)$ comes from the difference in initial distributions, and $l(t, X_t, u_t)$, is defined as

$$l(t, X_t, u_t) \triangleq g(t, X_t) + \frac{1}{2\epsilon} \|u_t\|^2 dt, \quad (8)$$

where $g(t, X_t), \Psi_T(x)$ are

$$\begin{aligned} g(t, X_t) &= \frac{1}{2\sigma_B^2} \|h(t, X_t)\|^2 dt + \frac{1}{\sigma_B^2} Y_t dh(t, X_t), \\ \Psi_T(x) &= -\frac{1}{\sigma_B^2} Y_T h(T, X_T). \end{aligned} \tag{9}$$

B. Hybrid Systems and the Linearization of Jump Dynamics

1. Hybrid Dynamical Systems

A Hybrid system, per [44], [45], is defined by the tuple: $\mathcal{H} := \{\mathcal{I}, \mathcal{D}, \mathcal{F}, \mathcal{G}, \mathcal{R}\}$, where:

- $\mathcal{I} := \{I_1, I_2, \dots, I_{N_I}\} \subset \mathbb{N}$ is a finite set of modes.
- $\Gamma \subset \mathcal{J} \times \mathcal{J}$ is the set of discrete transitions which form a directed graph structure over \mathcal{J}
- \mathcal{D} is the set of continuous domains which represent the state spaces, with pairings of nodes to modes (D_j, I_j) .
- \mathcal{F} is the set of flows which define the smooth dynamics F_j in each mode I_j
- $\mathcal{G} := \Pi_{(I,J) \in \Gamma} G_{(I,J)}(t)$ is the collection of guards where a specific $G_{(I,J)}(t) \subset D_I$ for each $(I, J) \in \Gamma$ is defined as a sublevel set of a C^r function.
- \mathcal{R} is the set of reset functions R_{jk} mapping the state from D_j to D_k when the guard condition G_{jk} is met.

We denote a transition from mode I_j to mode I_k happening at state $X_t^- := X(t^-)$ if the guard condition g_{jk}

$$g_{jk}(t^-, X_t^-) \leq 0, X_t^- \in I_j. \tag{10}$$

In turn, the jump dynamics are defined as

$$X_t^+ = R_{jk}(X_t^-) \in D_k, \tag{11}$$

where $R_{jk} \in \mathcal{R}$ is the corresponding reset function which maps between the two continuous domains when the guard condition g_{jk} is met. The notation (t^-, X_t^-) and (t^+, X_t^+) is used to represent the pre-impact and post-impact time-state pairs.

2. Stochastic Optimal Control with Hybrid Transitions

Let us define a controlled smooth flow in mode I_j as

$$dX_t^j = F_j(t, X_t^j)dt + \sigma_j(t, X_t^j)(u^j(t, X_t^j)dt + \sqrt{\epsilon}dW_t^j). \tag{12}$$

We define its corresponding uncontrolled flow, similar to Equation (1a), in this mode I_j as

$$dX_t^j = F_j(t, X_t^j)dt + \sigma_j(t, X_t^j)\sqrt{\epsilon}dW_t^j. \tag{13}$$

Now denote the period of $[t_j^+, t_{j+1}^-]$ to be in mode j , and denote the start and end period of this sequence as $[0, T]$. In other words

$$\begin{aligned} X_t^j &\in I_j, \forall t \in [t_j^+, t_{j+1}^-], \\ X^{j+1}(t_{j+1}^+) &= R_{j,j+1}(X^j(t_j^-)). \end{aligned} \quad (14)$$

Let us consider the stochastic optimal control problem over a series of different modes, as in [39]. Here, we identify the order of the hybrid transitions N_j prior to the simulation, causing its cost function to become

$$\min_u \mathcal{J} \triangleq \mathbb{E} \left[\sum_{j=0}^{N_j-1} \int_{t_j^+}^{t_{j+1}^-} l(t, X_t^j, u_t^j) + \Psi_T \right], \quad (15)$$

Now, let $F_{\Delta,i}^H(X_i^j, u_i)$ represent the hybrid transition for x from t_i to t_{i+1} . If the guard function $g_{j,j+1}(t_{i+1}, X_{t_{i+1}}) > 0$, then $X_{t_{i+1}}^j \in I_j$ is still in I_j , therefore

$$X_{t_{i+1}}^j = F_{\Delta,i}^H(X_i^j, u_i^j) \approx X_i^j + (F_j(t_i, X_i^j) + \sigma_j(X_i^j)u_i^j)\Delta t + \sigma_j(X_i^j)\Delta W_{t_i}^j. \quad (16)$$

On the other hand, if there is a jump at some $t_j^- \in [t_i, t_{i+1}]$, we approximate t_j^- as t_{i+1} , which holds up for substantially small timesteps. The hybrid dynamics with a jump are

$$X_{t_{i+1}}^{j+1} = F_{\Delta,i}^H(X_i^j, u_i^j) \approx R_{j,j+1}(X_i^j + F_j(t_i, X_i^j) + \sigma_j(X_i^j)u_i^j)\Delta t + \sigma_j(X_i^j)\Delta W_{t_i}^j. \quad (17)$$

III. Problem Formulation

We modify the path integral particle filter formulation [24] to apply it for the purpose of hybrid filtering. We apply the principles of hybrid path integral control from Equation (15). We will discuss hybrid smoothing, how to solve that problem through hybrid optimal control, and then extend the path integral formulation done in [24] and [39] to cover this area. For notation purposes, we frequently make use of j , which denotes "for specific-mode" in later contexts.

A. Smoothing for Hybrid Dynamical Systems

First, let us consider a standard diffusion process in the mode I_j . Similar to Equation (1a) and Equation (1b), the measurement $Y_t \in \mathbb{R}^P$ is corrupted by the standard Wiener process $B_t \in \mathbb{R}^P$

$$dX_t^j = F^j(t, X_t^j)dt + \sigma^j(t, X_t^j)\sqrt{\epsilon}dW_t^j, \quad X_0^j \sim \nu_0^j \quad (18a)$$

$$dY_t^j = H^j(t, X_t^j)dt + \sigma_B^j dB_t, \quad Y_0^j = 0. \quad (18b)$$

A transition from mode I_j to mode I_k happens in the dynamic state $X_t^- := X(t^-)$ as in Equation (19)

$$g_{jk}(t^-, X_t^-) \leq 0, X_t^- \in I_j. \quad (19)$$

Although the measurement Y_t is a nonlinear function of X_t , we assume that it shares the same mode, as would be consistent with an observation of a state. The jump dynamics are defined in the same way as Equation (11). Here, we do not assume that all of the modes follow the same noise distribution. Furthermore, there is a problem of potential mode mismatch between the nominal dynamics of a roll out and the computed posterior prediction, which we will discuss later. We assume that each mode is independent of the other before transitioning (so in turn there are independent, disjoint time intervals), which allows us to use the Pathwise Kallianpur-Striebel formula. For each mode, we are in a right-continuous space that has left-limits everywhere, per the definition of a càdlàg process. Therefore, we can use it summatively across all the modes, arriving at

$$\tilde{Z}_T \left(X_{[t_j^+, t_{j+1}^-]}, y \right) = \exp \left(\sum_{j=0}^{N_j} \left(H^j(X_T) \cdot Y_T^j - \int_{t_j^+}^{t_{j+1}^-} Y_t^j \cdot dH^j(X_t) - \frac{1}{2} \int_{t_j^+}^{t_{j+1}^-} \|H^j(X_t)\|^2 dt \right) \right). \quad (20)$$

As done previously, $\frac{dQ^Y}{d\mathcal{P}}$ is equivalent to $\tilde{Z}_T(X_{[0,T]}, y)$. Here, we can make the following substitution, for the purposes of simplifying notation

$$\tilde{Y}_t = \frac{Y_t^j}{\sigma_B^j}. \quad (21)$$

From there, substituting and plugging into Equation (20), we arrive at

$$\frac{dQ^Y}{d\mathcal{P}} \propto \exp \left(\sum_{j=0}^{N_j} \left\{ \left[\int_{t_j^+}^{t_{j+1}^-} \mathcal{L}^j(t, X_t, \tilde{Y}_t) \right] \right\} \right). \quad (22)$$

For future reference, we define the interior of the summation as the following "filtering cost per mode" \mathcal{L}_j

$$\mathcal{L}^j(t, X_t, Y_t) \triangleq -\frac{1}{\sigma_B^{j,2}} \left(Y_t^j dH^j + \frac{1}{2} \|H^j\|^2 dt - Y_T^j H^j(T, X_T) \right), \quad (23)$$

for the purpose of simplifying further analysis.

B. Solving Hybrid Filtering Through Hybrid Optimal Control

We now discuss how to apply Equation (15) into the context of the filtering problem from Equation (22). The key difference between this and our previous result for the control problem is that \mathcal{P}_u and \mathcal{P}_0 share the same initial distribution while \tilde{X}_0 and X_0 do not. Hence, the additional KL term denotes the differences in those initial distributions. Here, we can apply the result of Equation (4) and Equation (6) into the context of each individual hybrid mode. Plugging

those into Equation (22), we arrive at the following variational equation, for each mode

$$\mathbb{E}_{\tilde{P}} \left\{ \log \frac{d\tilde{P}}{dQ^Y} \right\} = \mathbb{E}_{\tilde{P}} \left\{ \int_{t_j^+}^{t_{j+1}^-} \frac{1}{2\epsilon} \|u_t\|^2 dt \right\} + KL(\pi_0^j \parallel \nu_0^j) - \mathbb{E}_{\tilde{P}} \left\{ \log \left(\exp \left\{ \int_{t_j^+}^{t_{j+1}^-} \mathcal{L}^j(t, X_t, Y_t) \right\} \right) \right\}. \quad (24)$$

Expanding this expression, we place it into our summation, and turn it into the equivalent minimization problem over the control input and initial distribution π_0 . The key note here though is that the problem involving minimizing the expectation from this initial distribution, the initial distribution is dependent on each state j . In other words, we can think of it as the problem of minimizing J independent noise distributions over each mode. We arrive at

$$\min_{u, \pi_0} \mathbb{E} \sum_{j=0}^{N_j} \left\{ \int_{t_j^+}^{t_{j+1}^-} \frac{1}{2\epsilon} \|u\|^2 dt - \mathcal{L}^j(t, X_t, Y_t) + KL(\pi_0^j \parallel \nu_0^j) \right\}. \quad (25)$$

In this equation, since we essentially define \tilde{X}_t as the expectation measure over \tilde{P} , we can replace X_t with this. We denote the resulting expression with this expectation measure as

$$\mathcal{J}_{\tilde{X}_t} = \sum_{j=0}^{N_j} \left\{ \int_{t_j^+}^{t_{j+1}^-} \frac{1}{2\epsilon} \|u\|^2 dt - \mathcal{L}^j(t, \tilde{X}_t, u) + KL(\pi_0^j \parallel \nu_0^j) \right\}. \quad (26)$$

Finally, now we can see the similarities between smoothing and optimal control, with comparing Equation (15) and Equation (26)

$$\min_u \mathbb{E} \sum_{j=0}^{N_j} \left\{ \int_{t_j^+}^{t_{j+1}^-} g(t, X_t) dt + \Psi_T(X_t^j) \right\} + \mathbb{E} \sum_{j=0}^{N_j} \left\{ \int_{t_j^+}^{t_{j+1}^-} \frac{1}{2\epsilon} \|u_t\|^2 \right\} \sim \min_{u, \pi_0} \mathbb{E} \left\{ \mathcal{J}_{\tilde{X}_t} \right\}. \quad (27)$$

Hence, we can see that if we write in terms of $g(t, x)dt$ and $\Psi_T(x)$, we get a similar result to Equation (9):

$$\begin{aligned} g(t, x)dt &= \frac{1}{2\sigma_B^2} \|H^j(t, x)\|^2 dt + \frac{1}{\sigma_B^2} Y_t^j dH^j(t, x), \\ \Psi_T(x) &= -\frac{1}{\sigma_B^2} Y_T^j H^j(T, x). \end{aligned} \quad (28)$$

Resubstituting to write into a more concise form as a function of this running and terminal cost, and by expressing the sum of the running and control cost as we did in Equation (8), we arrive at

$$\mathcal{J}_{\tilde{X}_{ot}} = \sum_{j=0}^{N_j} \left\{ \int_{t_j^+}^{t_{j+1}^-} l^j(t, X_t, u_t) + \Psi_T(X_t) + KL(\pi_0^j \parallel \nu_0^j) \right\}. \quad (29)$$

The only major difference between a finite-horizon stochastic hybrid optimal control problem in Equation (15), and Equation (29) is the extra term $KL(\pi_{j,0} \parallel \nu_{j,0})$. Now in the case that we have a mode mismatch between Y_t^j and X_t ,

whereas one of the following conditions is met

$$\begin{aligned} Y_t \in I_j, X_t \in I_{j+1} \\ X_t \in I_j, Y_t \in I_{j+1} \end{aligned} \quad (30)$$

This can be problematic, as several of the terms between Y_t and X_t depend on them being in the same mode. This was also discussed in [46] and [47], where it affected the feedback control law performance, similar to here. We use reference extensions to handle this case, as was done in [39], by dividing up the trajectory into two discretizations, each of which keep continuity: $[t_j^-, \dots, t_{N_f}]$ and $[t_1 \dots t_{N_b}, t_{j+1}^+]$, for the pre- and post- contact states. To compute the $Y_j dH_t$ terms, we use for the previous mode

$$x_{jN_f} \triangleq x(t_j^-) \cup \{Y_i^j\}_{i=1}^{N_f}, \forall i = 1 \dots N_f, \quad (31)$$

and likewise for the subsequent mode, we use

$$x_{j+1N_b} \triangleq x(t_{j+1}^+) \cup \{Y_i^{j+1}\}_{i=1}^{N_b}, \forall i = 1 \dots N_b. \quad (32)$$

This way, we keep continuity within that interval of transition, and avoid the comparison of a transitioned mode with that of an untransitioned mode.

C. Hybrid Path Integral Smoothing and Filtering

As was similar to [24], Equation (29) is different compared to Equation (15) from only the KL divergence term. In [39], the authors found that the optimal controller at time t , for Equation (15) could be expressed as (while ignoring the noise intensity terms, as those don't exist in our model)

$$u_t^* = \frac{\mathbb{E}_{\mathbb{P}^0} [\Delta W_t \exp(\mathcal{L}_H(t))]}{\Delta t \times \mathbb{E}_{\mathbb{P}^0} [\exp(\mathcal{L}_H(t))]}, \quad (33)$$

where $\mathcal{L}_H(t)$ is defined as the piecewise state cost:

$$\mathcal{L}_H(t) \triangleq \mathcal{I}_L [t, t_{j_m}^-] + \sum_{j=j_m}^{N_j} \mathcal{I}_L [t_j^+, t_{j+1}^-], \quad (34)$$

and j_m is the minimum j that $t_j^+ \geq t$ and \mathcal{I}_L is defined as

$$\mathcal{I}_L[a, b] \triangleq \int_a^b g(t, X_t) dt + \Psi_T(X_T^{N_j}). \quad (35)$$

We see that this optimal controller is independent of the distribution $\pi_{j,0}$. Plugging Eq. [33] into [29], we arrive at the optimization over $\pi_{j,0}$. Now, we use the following substitution to express the optimization over the initial distributions $\pi_{j,0}$:

$$V_t(x) = -\log \phi(t, x), \quad (36)$$

where $\phi(t, x)$ is defined as

$$\phi(t, x) = \mathbb{E}_{\mathbb{P}^0} [\exp(\mathcal{L}_H(t))]. \quad (37)$$

By splitting up the terms and applying properties of KL divergence, this causes our Eq. to simplify down to the following optimization problem which seeks to minimize the set of distributions $\pi_0 := \{\pi_{j,0}, \pi_{j+1,0}, \dots, \pi_{J,0}\}$

$$\min_{\pi_0} \mathbb{E} \left\{ \sum_{j=0}^{N_J} -\log \phi(0, X_0^j) - \log \nu_0^j(X_0^j) + \log \pi_0^j(X_0^j) \right\}. \quad (38)$$

Now, we can plug our controllable stochastic model, which will be how we run the rollout trajectories over X_t^j

$$dX_t^j = F_j(t, X_t^j)dt + \sigma^j(t, X_t^j)(u^j(t, X_t^j)dt + \sqrt{\epsilon}dW_t^j), \quad X_{0_j}^k \sim \pi_{0_j}^*, \quad (39)$$

into Equation (38), completing our optimal control setup.

D. Hybrid Particle Filtering

Now, we can apply the principles of particle filtering to this hybrid smoothing problem, analogous to how [24] did this with continuous-time systems. In doing so, we establish the key contribution of this paper: extending hybrid optimal control to particle filtering. First, we know the general equation for the conditional distribution of the signal X_t , given the measurement Y_t for $0 \leq t \leq T$ is

$$\frac{1}{K} \sum_{k=1}^K \delta_{X_t^k}. \quad (40)$$

Now, we can use Girsanov's theorem, and our standard KL divergence formula, which was also applied to continuous-time systems

$$\frac{dQ^Y}{d\tilde{\mathcal{P}}} = \frac{dQ^Y}{d\mathcal{P}} \frac{d\mathcal{P}}{d\tilde{\mathcal{P}}}. \quad (41)$$

By Girsanov theorem, and from Equation (22), we can come to that at a given mode, that Equation (41) is proportional to

$$\frac{dQ^Y}{d\mathcal{P}} \frac{d\mathcal{P}}{d\tilde{\mathcal{P}}} \propto \frac{d\nu_0}{d\pi_0} \exp[-S_u(0, T)], \quad (42)$$

where S_u is the mode-specific integral defined as

$$S_u(t, s) = \int_t^s \frac{1}{2\epsilon} \|u_\tau\|^2 d\tau - \mathcal{L}^j(\tau, X_\tau) + \frac{1}{\sqrt{\epsilon}} u'_\tau dW_\tau + \frac{1}{\sigma_B^2} Y_t(t, X_t). \quad (43)$$

We now define the weights, at a particular mode as

$$w_j^k = \frac{dv_0}{d\pi_0}(X_0^k) \exp[-S_u^k(t_j^+, t_{j+1}^-)]. \quad (44)$$

In the ‘‘Algorithm and Implementation’’ section, we discuss how we update the weights at the start of each new mode \mathcal{I}_j . From here, you can approximate dQ^Y . An empirical distribution is an estimate of the cumulative distribution function that generated the points in a sample. We can now combine the ideas used by the empirical distribution formula given by Equation (41), and use it to get the expression

$$dQ^Y \approx \sum_{k=1}^K \hat{w}_j^k \delta_{x_j^k}. \quad (45)$$

Here, \hat{w}^k is a normalized weight, a key factor to ensure that the state estimation stays effective, s.t.

$$\hat{w}_j^k = \frac{w_j^k}{\sum_{k=1}^K w_j^k}.$$

One can view the above expression as a weighted average that aims to approximate the posterior. Therefore, the posterior distribution for X_t^j for t s.t. $t_j^+ \leq t \leq t_{j+1}^-$ can be approximated by

$$\sum_{k=1}^K \hat{w}_{t_j}^k \delta_{X_{t_j}^k}. \quad (46)$$

Consider a sliding window $[t_j^+ - H, t]$ of size $H > 0$. We can take Equation (29), and modify it with this consideration, resulting in

$$\min_{u, \pi_0} \mathbb{E} \sum_{j=0}^{N_j} \left\{ \int_{t_j^+ - H}^t l^j(t, X_t, u_t) + \Psi_T(X_t) + KL(\pi_0^j \parallel v_0^j) \right\}, \quad (47)$$

We choose to use this approach in order to reduce the computational burden of this method. By doing so, we avoid stacking up recursive costs over time, and keep the runtime of the algorithm consistent over each iteration. While this may initially cut performance, we discuss later how with a proper size window, they can be mitigated, as was shown in [24]. Similarly to how we have done so earlier, we can represent these distributions as collections of weighted particles,

and using the sliding mode characteristic, we arrive at the following expression for the prior distribution,

$$v_{t-H} \approx \sum_{k=1}^K \tilde{w}_{t-H}^k \delta_{x_{t-H}^k}. \quad (48)$$

As was shown in [24], we compute a suboptimal control policy u for the closed-loop dynamics. From there, we compute our approximation of the posterior, through Equation (45). In other words, for prior and posterior weights, as in [24], we use the following two equations, respectively

$$\begin{aligned} \tilde{w}_{t_j^+ + H}^k &\propto \exp \left[-S_u^k(t_j^+, t_{j+1}^-) \right], \\ \hat{w}^k &\propto \exp \left[-S_u^k(t_j^+, t - H) \right] \exp \left[-S_u^k(t - H, t_{j+1}^-) \right] = \exp \left[-S_u^k(t_j^+, t_{j+1}^-) \right]. \end{aligned} \quad (49)$$

IV. Algorithm and Implementation

The reset map describing the mapping between pre-transition and post-transition modes $X_t^+ = R(t, X_t^-)$ is generally instant and nonlinear. Therefore, we use the Saltation Matrix, a first-order approximation for the varying effect of the transition along a nominal point [38, 48, 49], allowing for the preservation of continuity and differentiability. Given two modes j and k , the Saltation Matrix is defined as

$$\Xi_{jk} \triangleq \partial_x R_{jk} + \frac{F_k - \partial_x R_{jk} \cdot F_j - \partial_t R_{jk} \partial_x g_{jk}}{\partial_t g_{jk} + \partial_x g_{jk} \cdot F_j}. \quad (50)$$

With it, the dynamics of the perturbed state δX_t at hybrid transitions can be approximated as

$$\delta X_t^+ \approx \Xi_{jk} \delta X_t^-. \quad (51)$$

Notably, it has been proven to perform better than differentiating the reset map due to how it handles time differences upon hitting the guard condition [38]. This section provided details about how the PIPF algorithm was extended to hybrid systems and how the algorithm evaluates transition events. We assume constant step size discretization for this as well.

For our optimal control approach, we use a modified form of the Salted iLQR algorithm found in [36] to compute our feedback gains and resulting particle trajectories. This approach employs the Saltation Matrix to handle mode transitions in the backwards pass of the iLQR algorithm, allowing for smooth differentiation when computing the feedback gains if the system crosses modes. The main differences between our algorithm and the Salted iLQR algorithm lie in the computation of the running and terminal cost derivatives, as our problem is slightly different.

We also assume stochasticity in the modes, namely since the ground truth mode at a given point in time is not

known, each particle may not be in the same mode as the other. For estimation purposes under those conditions, we employ a form of “voting logic,” where we compare which mode has a greater overall particle weight. Once we identify which mode has a greater weight, the particles within that mode have their weights recomputed (so that they still sum to one), and we compute the state estimate using those particles.

The overall structure of the HPIPF algorithm is illustrated in Algorithm 1. We show the subroutine for an incoming measurement (one step of HPIPF step) over a time window in Algorithm 2. Lastly, we show an individual particle’s movement is propagated from a set of computed feedback and feedforward gains in Algorithm 3.

Algorithm 1 Hybrid Path Integral Particle Filtering (HPIPF)

Input: Total Number of Steps, Sliding Window and Sampling Frequency: (L, H, dt)
Sample Paths from Prior Distribution ν_0 : $\{\tilde{x}_p^k\}$
Weight of Prior Samples, Uniform: $\{\tilde{w}_p^k\}$
Modes in Prior Distribution: $\{\tilde{d}_p^k\}$
Output: State Trajectory Estimate, Mode Estimate (\bar{x}, \bar{d})
for $j = 1, \dots, L$ **do**
 j -th time interval $\leftarrow [\max(0, t_j - H), t_j]$
 $\{\hat{x}_j\}, \{\hat{w}_j\}, \{\hat{d}_j\}, \{\tilde{x}_{p,j}\}, \{\tilde{w}_{p,j}\}, \{\tilde{d}_{p,j}\} \leftarrow$ Algorithm 2 for j -th time interval
 $\bar{x}, \bar{d} \leftarrow$ Weighted averaging and voting logic
end for

Algorithm 2 One Step of HPIPF

Input: Cost: $C = \{g, \Psi\}$
Number of Particles, Sliding Window Size, Resampling Threshold: $\Phi = \{K, H, \gamma_{thres}\}$
Prior Samples, Weights, Modes: $\mathcal{P}_{sample} = \{\tilde{x}_{p,j}, \tilde{w}_{p,j}, \tilde{d}_{p,j}\}$
Output: Filtering (Posterior) Results: $\{\hat{x}_j, \hat{w}_j, \hat{d}_j\}$
Updated Sampling (Prior) Results: $\{\tilde{x}_{p,j}, \tilde{w}_{p,j}, \tilde{d}_{p,j}\}$
Inputs for Computing Gains: \mathcal{X}, \mathcal{M}
 $k_{feedforward}, K_{feedback} \leftarrow$ Solve Hybrid iLQR (47)
for $k \leftarrow 1, \dots, K$ **do**
 $\{\hat{x}^k\}, \{\hat{w}^k\}, \{\hat{d}^k\}, \{\tilde{x}_p^k\}, \{\tilde{w}_p^k\}, \{\tilde{d}_p^k\} \leftarrow$ Algorithm 3
 Normalize sample and filtering weights (\tilde{w}_j, \hat{w}_j)
end for
Check resampling:
Effective ratio: $\gamma = \frac{1}{K \sum_{k=1}^K (\hat{w}^k)^2}$
if $\gamma < \gamma_{thres}$ **then**
 $\{\tilde{x}_p^k\} \sim$ multinomial $(\{\tilde{x}_{t_j}^k\}, \{\tilde{w}^k \exp(-S_u^k(t_i, t_j))\})$
 $\{\tilde{w}_p^k\} \propto \exp(S_u^k(t_i, t_j))$
 $\{\tilde{d}_p^k\} \leftarrow$ Mode \tilde{d}^k at \tilde{x}_p^k
end if

Algorithm 3 One Step of the Particle Update in PIPF Step

Input: Particle to Sample: k

Cost: $C = \{g, \Psi\}$

Number of Particles, Sliding Window Size, Resampling Threshold: $\Phi = \{K, H, \gamma_{thres}\}$

Prior Samples, Weights, Modes: $\mathcal{P}_{sample} = \{\tilde{x}_{p,j}, \tilde{w}_{p,j}, \tilde{d}_{p,j}\}$

Current Feedforward, Feedback Gains: $(k_{feedforward}, K_{feedback})$

Output: Filtering (Posterior) Results: $\{\hat{x}_j^k, \hat{w}_j^k, \hat{d}_j^k\}$

Updated Sampling (Prior) Results: $\{\tilde{x}_p^k, \tilde{w}_p^k, \tilde{d}_p^k\}$

Compute control inputs using computed gains, sample k -th trajectory X_j^k initialized by X_p^k with (39)

while time evolves over $[t_i, t_j]$ **do**

 Propagate \mathbf{x}_k using $F_{d_k}(x, u)$

if \mathbf{x}_k crosses a guard $g_{d_k d_l}(x) = 0$ **then**

 Transition to domain d_l using reset map

$\mathbf{x}_k \leftarrow R_{d_k d_l}(\mathbf{x}_k)$

 Update domain index: $d_k \leftarrow d_l$

end if

end while

Use reference extensions to extract the points of the shared mode between the reference trajectory and the measurement (31), (32)

Evaluate the value of S_u^k over the trajectory X_j^k , modes $d_{t_j}^k$ (43)

Filtering samples, modes: $X^k = X_{t_j}^k, d^k = d_{t_j}^k$

Filtering weight: $\hat{w}_j^k \propto \tilde{w}_p^k \exp(-S_u^k(t_i, t_j))$ (49)

Prior information for usage in next sliding window

Prior sample, mode: $\tilde{x}_p^k = X_{t_i+1}^k, \tilde{d}_p^k = d_{t_i+1}^k$

Prior sampling weight: $\tilde{w}_p^k \propto \tilde{w}_{t_i}^k \exp(-S_u^k(t_i, t_i + 1))$ (49)

V. Numerical Examples and Results

In this section, we present two numerical examples to demonstrate the working of the algorithm and compare the accuracy with respect to the exact posterior distribution. We consider two systems for this: (1) Bouncing Ball System and (2) Spring Loaded Inverted Pendulum. Each system is set up to transition exactly once approximately midway through the time sequence. By default, we set $dt = 0.01$, $K = 50$, $H = 10$, $\epsilon = 0.1$, while for SLIP, the defaults are $dt = 0.001$, $K = 100$, $\epsilon = 0.01$. We test using Gaussian noise as there is a closed-form known posterior (the SKF), under the expectation that a particle filter's inherent flexibility will allow performance to translate.

All the systems considered have at least one hybrid event in their dynamics (of which the timing is unknown to the algorithm). The first step is to calculate the true posterior of the systems. The SKF [37] was used to estimate the true posterior, as we simulate our system with Gaussian noise (under the expectation that performance can hence be extended to non-Gaussian noise, which may not have closed-form posteriors). The results from the posterior estimate using SPIPF were then compared against this and the time-averaged mean squared error (which we refer to as Mean MSE) was calculated. Experiments were conducted based on (a) Number of particles used for simulation K , (b) the time discretization dt , and (c) the sliding window size H (which were found to be contributing factors in performance from [24] and [40]).

The Mean MSE was defined as the following additive expression

$$\text{Mean MSE} = \frac{1}{N} \sum_{n=1}^N \left((x(t_n) - \hat{x}(t_n))^T (x(t_n) - \hat{x}(t_n)) \right), \quad (52)$$

where N is the number of time steps, $\hat{x}(t_n)$ is the state estimate at time t_n , and $x(t_n)$ is the true state at time t_n . For each measurement noise, process noise, and time step combination, the filter is run on randomly sampled starting conditions with randomly sampled process noise and randomly sampled measurements.

We test our algorithm against two baselines: a Sequential Importance Resampling (SIR) Multi-Mode Particle Filter (employing the same previously mentioned voting logic for deciding particle mode), as well as a modified form of our algorithm that uses 0-control. We present this ablation (0-control) in comparison to our approach in the results below.

A. Bouncing Ball System

We also simulated a 1-D bouncing ball under elastic impact [29]. This example can be viewed as a simplified and structurally homogeneous case of the Tensegrity robot [11] or other landing systems. States that were considered were the position and velocity. Guard sets were defined with respect to the velocity such that the domain of F_1 is when the velocity is negative (falling down) and the domain of F_2 is when the velocity is positive (bouncing back up). The guard conditions here are defined as

$$\dot{x} > 0 \quad \text{and} \quad \dot{x} < 0, \quad \text{where } \mathbf{x} = \begin{bmatrix} x_1 \\ x_2 \end{bmatrix} = \begin{bmatrix} x \\ \dot{x} \end{bmatrix}. \quad (53)$$

We show a visualization of this system below in Fig. 2.

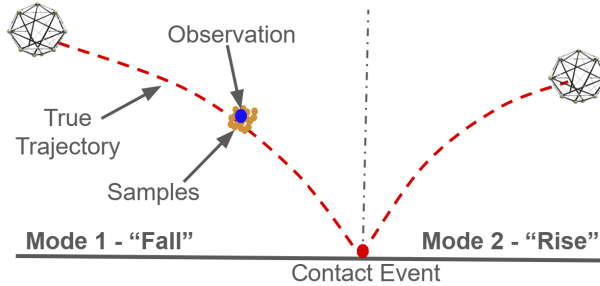


Fig. 2 Bouncing Ball Visualization

Now, the dynamics for each mode required a "simulated" control input in this case as we were essentially solving an iLQR problem for each time window of the PIPF algorithm. So the dynamics are given as

$$F_1(x, u) = F_2(x, u) := \begin{bmatrix} \dot{x} \\ \frac{u-mg}{m} \end{bmatrix} + \sqrt{\epsilon} \begin{bmatrix} 0 \\ \frac{1}{m} \end{bmatrix} dW_t^{(1,2)}. \quad (54)$$

Hybrid mode 1 transitions to 2 when the ball hits the ground, $g_{1,2}(x) := x$, and mode 2 transitions to 1 at $g_{2,1}(x) := \dot{x}$. When mode 1 transitions to 2, an elastic impact is applied, with a coefficient of restitution $-e$. The reset map from 2 to 1 is identity.

The Jacobian of the reset map and saltation matrix are

$$D_x R_{1,2} = \begin{bmatrix} 1 & 0 \\ 0 & -e \end{bmatrix}, \quad \Xi_{1,2} = \begin{bmatrix} 1 & 0 \\ \frac{-e(u-mg)(e+1)}{mz^2} & -e \end{bmatrix}. \quad (55)$$

B. Spring Loaded Inverted Pendulum (SLIP) System

The last system considered was the SLIP System. This system is used to model bipedal or quadrupedal robots for their locomotion. This system was included and useful to analyze since it involves both nonlinear dynamics and non-identity reset maps. We establish the point mass m , and leg with a spring constant k and original length r_0 . We define the following as the overall system's state vector $\{p_x, v_x, p_z, v_z, \theta, \dot{\theta}, r, \dot{r}\}$. Here, (p_x, p_z) are the horizontal and vertical positions of the body, (v_x, v_z) are the respective velocities, $\theta, \dot{\theta}$ are the angle and its respective velocity component between the body and the ground, and r, \dot{r} are the leg length and the changing rate.

This system consists of two modes, $\mathcal{I} = \{I_1, I_2\}$, where I_1 is the *flight mode* $I_1 \triangleq \{X_t^1 | p_z - r_0 \sin \theta \geq 0\}$, and I_2 is the *stance mode* $I_2 \triangleq \{X_t^2 | p_z - r_0 \sin \theta < 0\}$. Due to how we use a polar setup for the stance mode, there are different state spaces for each of the two systems. We visualize the system below in Fig. 3:

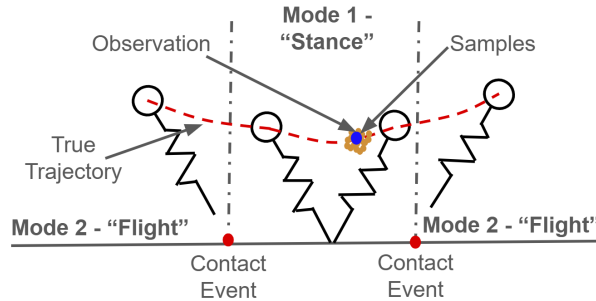


Fig. 3 SLIP Visualization

In the flight mode, the state space and smooth flow are defined as follows:

$$\begin{aligned}
X_t^1 &= \begin{bmatrix} p_x & v_x & p_z & v_z & \theta \end{bmatrix}, \\
dX_t^1 &= \begin{pmatrix} \begin{bmatrix} \dot{v}_x \\ 0 \\ \dot{v}_z \\ -g \\ 0 \end{bmatrix} + \begin{bmatrix} 0 \\ u_{1,t}^1 \\ 0 \\ u_{2,t}^1 \\ u_{3,t}^1 \end{bmatrix} \\ dt + \begin{bmatrix} 0 & 0 & 0 \\ 1 & 0 & 0 \\ 0 & 0 & 0 \\ 0 & 1 & 0 \\ 0 & 0 & 1 \end{bmatrix} dW_t^1, \end{pmatrix} \tag{56}
\end{aligned}$$

where g is the gravity, and we assume the system has control of its body and leg velocities. On the other hand, in the stance mode, the state space and smooth flow are defined as

$$\begin{aligned}
X_t^2 &= \begin{bmatrix} \theta & \dot{\theta} & r & \dot{r} \end{bmatrix}, \\
dX_t^2 &= \begin{pmatrix} \begin{bmatrix} \dot{\theta} \\ \frac{-3\dot{\theta}\dot{r}-g\times\cos\theta}{r} \\ \dot{r} \\ \frac{k(r_0-r)}{m} - g \sin\theta + \dot{\theta}^2 r \end{bmatrix} + \begin{bmatrix} 0 \\ 0 \\ \frac{m}{r^2} u_{1,t}^2 \\ \frac{k}{m} u_{2,t}^2 \end{bmatrix} \\ dt + \begin{bmatrix} 0 & 0 \\ 0 & 0 \\ \frac{m}{r^2} & 0 \\ 0 & \frac{k}{m} \end{bmatrix} \begin{bmatrix} dW_{1,t}^2 \\ dW_{2,t}^2 \end{bmatrix}. \end{pmatrix} \tag{57}
\end{aligned}$$

We define the reset maps between the two modes as

$$X_{t^+}^2 = R_{12}(X_{t^-}^1) = \begin{bmatrix} \theta^- \\ \frac{p_x^- v_z^- - p_z^- v_x^-}{r_0^2} \\ r_0 \\ -v_x^- \cos\theta^- + v_z^- \sin\theta^- \end{bmatrix}, \tag{58a}$$

$$X_{t^+}^1 = R_{21}(X_{t^-}^2) = \begin{bmatrix} p_{x,T}^- + r_0 \cos\theta^- \\ \dot{r}^- \cos\theta^- - r^- \dot{\theta}^- \sin\theta^- \\ r_0 \sin\theta^- \\ r_0 \dot{\theta}^- \cos\theta^- + \dot{r}^- \sin\theta^- \\ \theta^- \end{bmatrix}, \tag{58b}$$

where we assume $p_{x,T}$ is the pole x -position, and goes unchanged in the stance mode. In the monopedal hopping quadcopter developed in [50], a similar set of hybrid modes (with modified dynamics) were also used.

VI. Results

A. Bouncing Ball

The bouncing ball system is fairly linear, and therefore we can get solid estimation results by using a lower amount of particles. In our first set of results, we study the impact of changing K on mode prediction, MSE, and effective sample size (ESSE).

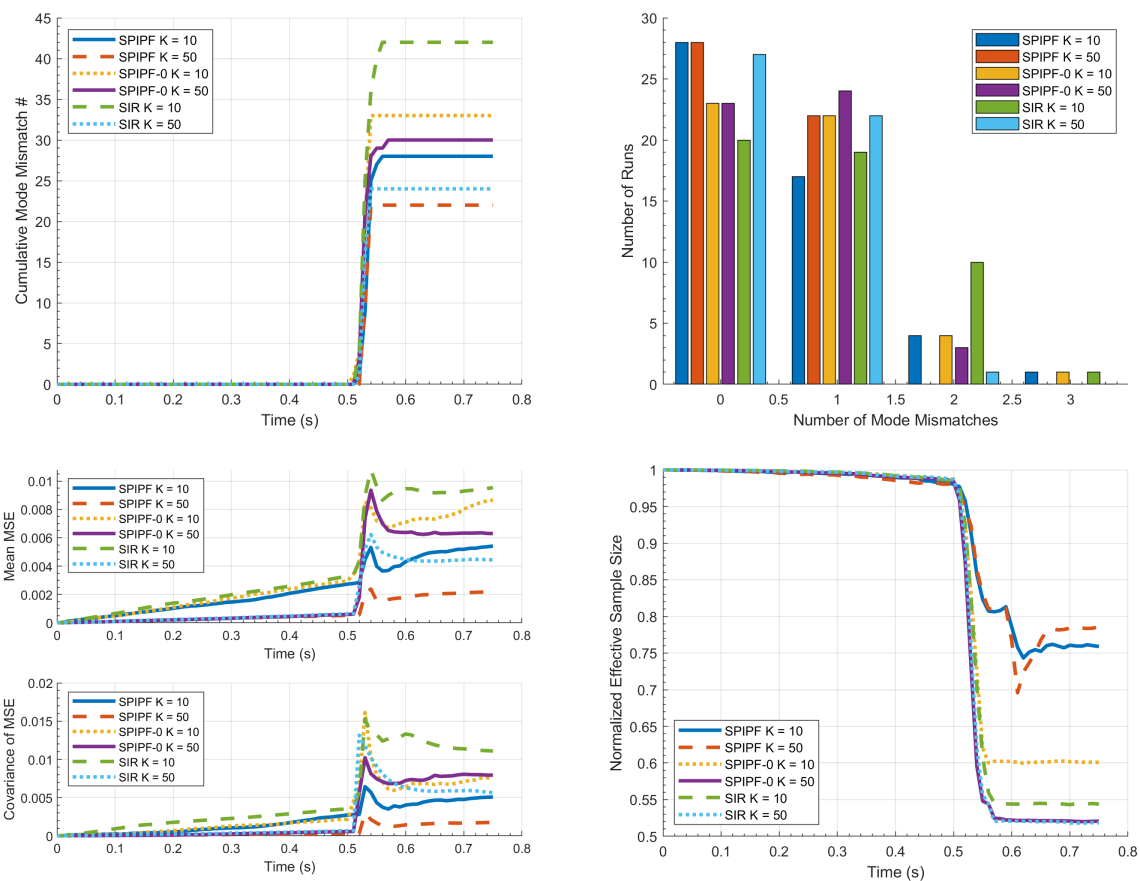


Fig. 4 Results from Changing Particle Count

As can be seen, our method significantly outperforms our baselines (SPIPF-0, and SIR), for all particle counts after the transition. Notably, our approach with 10 particles is better than the baselines, even when they use 50 particles. With 50 particles on our approach, we see higher mode prediction accuracy versus 10 particles, with an interesting tradeoff of lower ESSE. Note that the ESSE is still well-above our resampling threshold. One interesting characteristic is the dip in ESSE around 0.1 seconds after the transition. This makes sense, as per our sliding window logic, the particles at 0.1

seconds after the transition would be either initialized in mode 1 or 2, depending on the prior, which would cause a sharp deviance in particle weight at that point.

On the other hand, the histogram plot involving mode mismatches is less conclusive. We believe in the presence of stochasticity, these results are not incredibly useful to interpret, so long as the mode accuracy is within 0.2 seconds.

Next, we vary the size of the sliding window H , and show the results below for 10 particles.

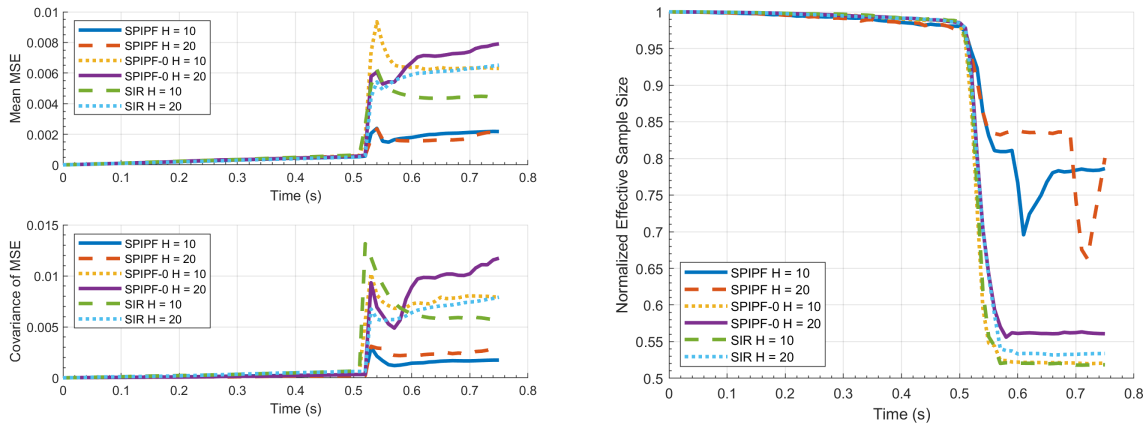


Fig. 5 Results from Changing Sliding Window Size

As expected, our model again outperforms the baseline, and with a higher sliding window size, we see more accuracy and lower covariance with respect to the MSE. This is expected as that increases the window that our algorithm looks backward. Again, we posit the same root cause for the dip in ESSE in the graph of $H = 20$, but this aligns with 0.2 seconds after transition (which again makes sense as that is 20 timesteps after the transition).

Now, we look at results as we vary the timestep dt .

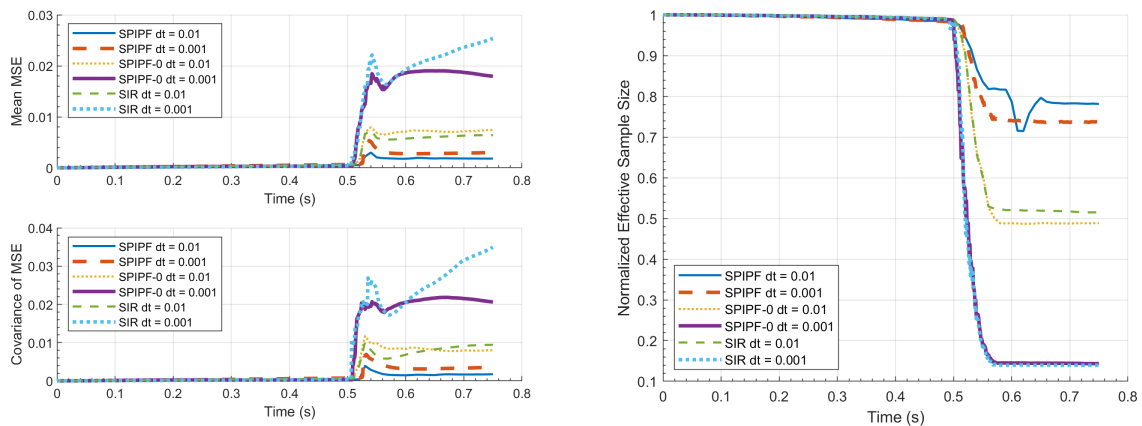


Fig. 6 Results from Changing Algorithm Timestep

Here, with a lower algorithm timestep, we actually see our algorithm (top left graph, orange line), substantively

outperforms our baselines when it comes to mode prediction. At the same time, we see the dip in ESSE we previously saw from being near a sample window almost disappearing completely, which makes sense as the smaller timestep should reduce those perturbations. At the same time, we see somewhat minimal differences in Mean MSE and Covariance of MSE, as expected due to the linearity and simplicity of our system.

B. SLIP System

Numerical simulation was carried out using MATLAB for the aforementioned systems with at least one hybrid event. As stated earlier, we present results for $\epsilon = 0.01, dt = 0.001$. Since we showed the relationship between algorithm timestep in the results for bouncing ball, we solely stick to the results associated with particle count and sliding window size in this analysis. We also do not allow for resampling in our method here either. Our results are below:

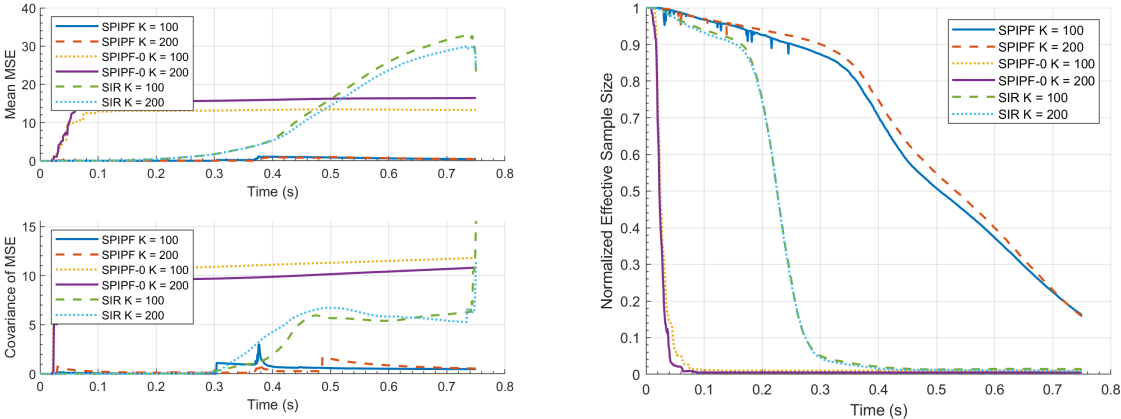


Fig. 7 Results from Changing Particle Size with SLIP System

From the results shown in Fig. 7, we can see that our algorithm outperforms the baseline methods with respect to Effective Sample Size throughout, both before and after the transition (which happens in the region of 0.35 seconds). Furthermore, we see substantively lower MSE values across both mean and covariance. As the system was highly unstable, we thresholded our results to only include the simulations that yielded below a certain MSE (which was set to 50), providing a similar number of trials per algorithm. Lastly, we see that our method also reports substantively lower MSE covariance than the two baselines we compare against. Next, we vary the sliding window size across the trials, and obtain further results, as shown below in Fig. 8.

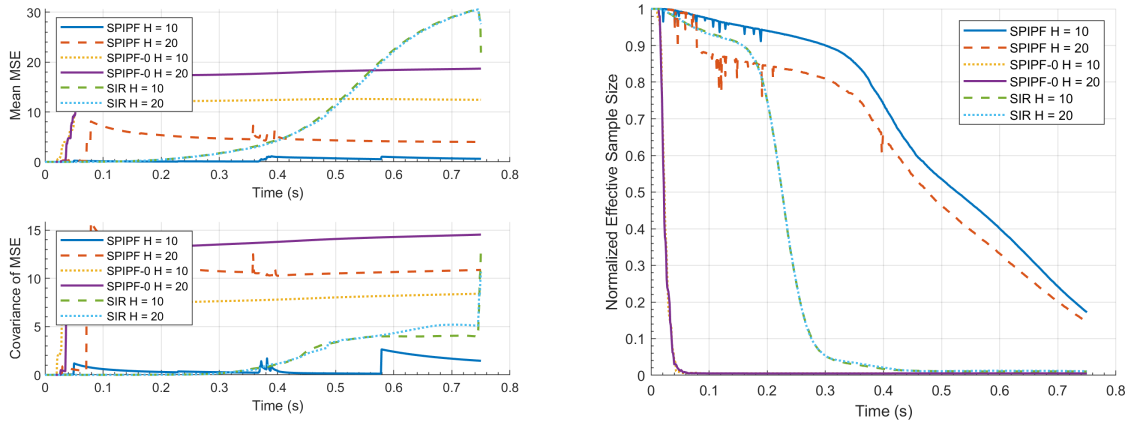


Fig. 8 Results from Changing Sliding Window Size with SLIP System

Namely, we find it interesting that increasing the sliding window size does not necessarily yield improved performance. We believe that this has to do with the overall instability of the system, and in analysis of specific simulations, we found that our approach (specifically in this case, but it was also found in the baselines), could predict a variety of simulation times, around ± 0.1 seconds before or after the actual transition occurred (which was set to be around 0.35 seconds). We believe this has to do with the instability of the system with respect to transitions, and during a longer sliding window, the system ends up triggering transitions earlier (which can be seen in the increased number of downward spikes in the effective sample size plot). This in turn suggests a high sensitivity to guard detection in the analysis of this system.

VII. Conclusion

A. Summary on Current Work

In our work, we extended prior work into path integral particle filtering to be applied to hybrid systems by using the linearization properties given by Saltation Matrices. Our work allows for non-Gaussian state estimation for hybrid systems with an optimal control approach, enabling for reduction of weight degeneracy, and a higher robustness against outlier measurement information. Using the Mean MSE metric and the SKF as our baseline, we found that our method consistently achieved higher estimation accuracy on both the bouncing ball and SLIP systems. Parallelizing the simulation in MATLAB yielded a speedup of 6X (because the laptop used to run experiments had 6 CPU cores), enabling large-scale experiments to be run efficiently. Finally, introducing reference-trajectory extensions significantly enhanced estimation performance near mode transitions.

B. Future Steps

Through our paper, we have shown the successful implementation of a mode-agnostic particle filtering algorithm for estimation of contact dynamics. We see future work in this area as pursuing two further veins: the exploitation of

parallelization properties of our algorithm, and active testing on hardware. Firstly, our algorithm has heavy promise for the use of multithreading, as after the initial optimal control problem is solved, and control gains are computed, the trajectories can be simulated on separate threads (and they all run for similar periods of time). This has been explored in [51] and [52]. [52] focuses on accelerating the resampling stage for GPU execution whereas [51] studies the redistribution of particles using OpenMP 4.5. Future work for our method should explore parallel implementations where particle propagation and resampling are designed to avoid idle workers. In particular, adaptive redistribution of particle rollouts after resampling—assigning compute based on per-particle simulation cost—could improve efficiency for systems with frequent event based transitions.

Secondly, we see potential interesting applications with hardware; contact dynamics are difficult to model, but promise has been seen learning methods for system identification [53]. Our algorithm could take such a plant model, in the form of Jacobians, and properly apply it to active online estimation, comparing with traditional approaches such as impact-aware Kalman filters [54], as well as the SKF [37]. This algorithm could also be applied to for state estimation in jumping real-world systems such as the Super Ball-Bot experiment at NASA [55] or orbital debris capture [13].

Acknowledgment

This material is based upon work supported by the National Science Foundation Graduate Research Fellowship Program under Grant No. DGE-2039655. Any opinions, findings, and conclusions or recommendations expressed in this material are those of the author(s) and do not necessarily reflect the views of the National Science Foundation.

References

- [1] Kalman, R. E., “A New Approach to Linear Filtering and Prediction Problems,” *Journal of Basic Engineering*, Vol. 82, No. 1, 1960, pp. 35–45. <https://doi.org/10.1115/1.3662552>.
- [2] Julier, S. J., and Uhlmann, J. K., “A New Extension of the Kalman Filter to Nonlinear Systems,” *Proceedings of AeroSense: The 11th International Symposium on Aerospace/Defense Sensing, Simulation and Controls*, SPIE, Orlando, FL, USA, 1997, pp. 182–193.
- [3] Julier, S. J., and Uhlmann, J. K., “Unscented Filtering and Nonlinear Estimation,” *Proceedings of the IEEE American Control Conference*, Albuquerque, NM, USA, 1995, pp. 1628–1632.
- [4] Giannitrapani, A., Ceccarelli, N., Scortecci, F., and Garulli, A., “Comparison of EKF and UKF for Spacecraft Localization via Angle Measurements,” *IEEE Transactions on Aerospace and Electronic Systems*, Vol. 47, No. 1, 2011, pp. 75–84. <https://doi.org/10.1109/TAES.2011.5705660>.
- [5] Qi, D., Feng, J., Ni, X., and Wang, L., “Maximum Correntropy Extended Kalman Filter for Vehicle State Observation,” *International Journal of Automotive Technology*, Vol. 24, No. 3, 2023, pp. 377–388. <https://doi.org/10.1007/s12239-023-0031-8>, URL <https://doi.org/10.1007/s12239-023-0031-8>.

- [6] Zhao, H., Tian, B., and Chen, B., “Robust stable iterated unscented Kalman filter based on maximum correntropy criterion,” *Automatica*, Vol. 142, 2022, p. 110410. <https://doi.org/https://doi.org/10.1016/j.automatica.2022.110410>, URL <https://www.sciencedirect.com/science/article/pii/S0005109822002631>.
- [7] Zhao, H., Horn, J., Reher, J., Paredes, V., and Ames, A. D., “Multicontact Locomotion on Transfemoral Prostheses via Hybrid System Models and Optimization-Based Control,” *IEEE Transactions on Automation Science and Engineering*, Vol. 13, No. 2, 2016, pp. 502–513. <https://doi.org/10.1109/TASE.2016.2524528>.
- [8] Koval, M. C., Dogar, M., Pollard, N., and Srinivasa, S., “Pose Estimation for Planar Contact Manipulation with Manifold Particle Filters,” *The International Journal of Robotics Research*, 2015.
- [9] Payne, J. J., “State Estimation Techniques for Hybrid Dynamical Systems,” Ph.D. thesis, Mechanical Engineering Department, Carnegie Mellon University, Pittsburgh, PA, September 2024.
- [10] SunSpiral, V., Agogino, A., and Atkinson, D., “Super Ball Bot – Structures for Planetary Landing and Exploration, NIAC Phase 2 Final Report,” Technical Report ARC-E-DAA-TN27344, NASA Ames Research Center, September 2015. URL <https://ntrs.nasa.gov/citations/20160000577>.
- [11] Garanger, K., del Valle, I., Rath, M., Krajewski, M., Sabelhaus, A. P., SunSpiral, V., and Agogino, A., “Soft Tensegrity Systems for Planetary Landing and Exploration,” *Earth and Space 2021: Space Exploration, Utilization, Engineering, and Construction in Extreme Environments*, American Society of Civil Engineers (ASCE), 2021, pp. 841–854. <https://doi.org/10.1061/9780784483374.078>.
- [12] Saranathan, H., and Grant, M. J., “Relaxed Autonomously Switched Hybrid System Approach to Indirect Multi-Phase Trajectory Optimization for Aerospace Vehicles,” *Journal of Spacecraft and Rockets*, Vol. 55, No. 3, 2018, pp. 534–546. <https://doi.org/10.2514/1.A34012>.
- [13] Soderlund, A. A., and Phillips, S., “Hybrid Systems Approach to Autonomous Rendezvous and Docking of an Underactuated Satellite,” *Journal of Guidance, Control, and Dynamics*, Vol. 46, No. 10, 2023, pp. 1901–1918. <https://doi.org/10.2514/1.G006813>, URL <https://doi.org/10.2514/1.G006813>.
- [14] Gordon, N. J., Salmond, D. J., and Smith, A. F. M., “Novel Approach to Nonlinear/Non-Gaussian Bayesian State Estimation,” *IEE Proceedings F - Radar and Signal Processing*, Vol. 140, No. 2, 1993, pp. 107–113. <https://doi.org/10.1049/ip-f-2.1993.0015>.
- [15] Kitagawa, G., “Monte Carlo Filter and Smoother for Non-Gaussian Nonlinear State Space Models,” *Journal of Computational and Graphical Statistics*, Vol. 5, No. 1, 1996, pp. 1–25. <https://doi.org/10.1080/10618600.1996.10474692>.
- [16] Del Moral, P., “Nonlinear filtering: Interacting particle resolution,” *Comptes Rendus de l’Académie des Sciences - Series I - Mathematics*, Vol. 325, 1997, pp. 653–658.
- [17] Murata, M., Kawano, I., and Inoue, K., “Degeneracy-Free Particle Filter: Ensemble Kalman Smoother Multiple Distribution Estimation Filter,” *IEEE Transactions on Automatic Control*, Vol. 67, No. 12, 2022, pp. 6956–6961. <https://doi.org/10.1109/TAC.2022.3185007>.

- [18] Fox, D., “KLD-Sampling: Adaptive Particle Filters,” *Neural Information Processing Systems*, 2001, pp. 1–8. URL <https://api.semanticscholar.org/CorpusID:10171391>.
- [19] Elvira, V., Míguez, J., and Djurić, P. M., “Adapting the Number of Particles in Sequential Monte Carlo Methods Through an Online Scheme for Convergence Assessment,” *IEEE Transactions on Signal Processing*, Vol. 65, 2015, pp. 1781–1794. URL <https://api.semanticscholar.org/CorpusID:10625542>.
- [20] Snyder, C., Bengtsson, T., Bickel, P., and Anderson, J., “Obstacles to High-Dimensional Particle Filtering,” *Monthly Weather Review*, Vol. 136, No. 12, 2008, pp. 4629 – 4640. <https://doi.org/10.1175/2008MWR2529.1>, URL <https://journals.ametsoc.org/view/journals/mwre/136/12/2008mwr2529.1.xml>.
- [21] Kim, J. W., and Mehta, P. G., “An Optimal Control Derivation of Nonlinear Smoothing Equations,” *Advances in Dynamics, Optimization and Computation*, Springer, 2020, pp. 295–311. https://doi.org/10.1007/978-3-030-51264-4_12.
- [22] Stengel, R. F., *Optimal control and estimation*, Dover books on advanced mathematics, Dover Publications, 1994.
- [23] Djuric, P., Kotecha, J., Zhang, J., Huang, Y., Ghirmai, T., Bugallo, M., and Miguez, J., “Particle filtering,” *IEEE Signal Processing Magazine*, Vol. 20, No. 5, 2003, pp. 19–38. <https://doi.org/10.1109/MSP.2003.1236770>.
- [24] Zhang, Q., Taghvaei, A., and Chen, Y., “An optimal control approach to particle filtering,” *Automatica*, Vol. 151, 2023, p. 110894. <https://doi.org/https://doi.org/10.1016/j.automatica.2023.110894>, URL <https://www.sciencedirect.com/science/article/pii/S0005109823000444>.
- [25] Back, J. A., Guckenheimer, J. M., and Myers, M., “A Dynamical Simulation Facility for Hybrid Systems,” *Hybrid Systems, Lecture Notes in Computer Science*, Vol. 736, Springer Berlin/Heidelberg, Berlin, Heidelberg, 1993, pp. 255–267.
- [26] Bledt, G., Wensing, P. M., Ingersoll, S., and Kim, S., “Contact Model Fusion for Event-Based Locomotion in Unstructured Terrains,” *2018 IEEE International Conference on Robotics and Automation (ICRA)*, IEEE, 2018, pp. 4399–4406. <https://doi.org/10.1109/ICRA.2018.8462872>.
- [27] Zhang, J., Pace, A. M., Burden, S. A., and Aravkin, A., “Offline State Estimation for Hybrid Systems via Nonsmooth Variable Projection,” *Automatica*, Vol. 115, 2020, p. 108871. <https://doi.org/10.1016/j.automatica.2020.108871>.
- [28] Lygeros, J., Johansson, K., Simic, S., Zhang, J., and Sastry, S., “Dynamical properties of hybrid automata,” *IEEE Transactions on Automatic Control*, Vol. 48, No. 1, 2003, pp. 2–17. <https://doi.org/10.1109/TAC.2002.806650>.
- [29] Goebel, R., Sanfelice, R. G., and Teel, A. R., “Hybrid dynamical systems,” *IEEE Control Systems Magazine*, Vol. 29, No. 2, 2009, pp. 28–93. <https://doi.org/10.1109/MCS.2008.931718>.
- [30] Sarkka, S., and Solin, A., *Applied Stochastic Differential Equations*, Cambridge Press, 2019.
- [31] Swonder, D. D., and Boyd, J. E., *Estimation Problems in Hybrid Systems*, Cambridge University Press, 1999.

- [32] Skaff, S., Rizzi, A. A., Choset, H., and Lin, P.-C., “The interacting multiple model algorithm for systems with Markovian switching coefficients,” *IEEE Transactions on Automatic Control*, Vol. 33, No. 8, 1988, pp. 780–783. <https://doi.org/10.1109/9.1299>.
- [33] Blom, H., and Bar-Shalom, Y., “The interacting multiple model algorithm for systems with Markovian switching coefficients,” *IEEE Transactions on Automatic Control*, Vol. 33, No. 8, 1988, pp. 780–783. <https://doi.org/10.1109/9.1299>.
- [34] Hwang, I., Balakrishnan, H., and Tomlin, C., “State estimation for hybrid systems: Applications to aircraft tracking,” *IEE Proceedings - Control Theory and Applications*, Vol. 152, No. 5, 2005, pp. 563–573. <https://doi.org/10.1049/ip-cta:20050053>, iEE Proceedings online no. 20050053.
- [35] Leine, R. I., and Nijmeijer, H., *Dynamics and Bifurcations of Non-Smooth Mechanical Systems*, Vol. 18, Springer Science & Business Media, 2013. <https://doi.org/10.1007/978-3-642-56402-6>.
- [36] Kong, N. J., Council, G., and Johnson, A. M., “iLQR for Piecewise-Smooth Hybrid Dynamical Systems,” *2021 60th IEEE Conference on Decision and Control (CDC)*, 2021, pp. 5374–5381. <https://doi.org/10.1109/CDC45484.2021.9683506>.
- [37] Kong, N. J., Payne, J. J., Council, G., and Johnson, A. M., “The Salted Kalman Filter: Kalman filtering on hybrid dynamical systems,” *Automatica*, Vol. 131, 2021, p. 109752. <https://doi.org/https://doi.org/10.1016/j.automatica.2021.109752>, URL <https://www.sciencedirect.com/science/article/pii/S0005109821002727>.
- [38] Kong, N. J., Payne, J. J., Zhu, J., and Johnson, A. M., “Saltation Matrices: The Essential Tool for Linearizing Hybrid Dynamical Systems,” , 2023.
- [39] Yu, H., Franco, D. F., Johnson, A. M., and Chen, Y., “Path Integral Control for Hybrid Dynamical Systems,” *arXiv preprint arXiv:2411.00659*, 2024. URL <https://arxiv.org/abs/2411.00659>, accessed: 2024-12-12.
- [40] Yuan, B., Zhang, Q., and Chen, Y., “An Optimal Control Approach to Particle Filtering on Lie Groups,” *IEEE Control Systems Letters*, Vol. 7, 2023, pp. 1195–1200. <https://doi.org/10.1109/LCSYS.2022.3232562>.
- [41] van Handel, R., “Filtering, Stability, and Robustness,” Ph.D. thesis, California Institute of Technology, 2007.
- [42] Kim, J. W., and Mehta, P. G., “An Optimal Control Derivation of Nonlinear Smoothing Equations,” *Advances in Dynamics, Optimization and Computation*, edited by O. Junge, O. Schütze, G. Froyland, S. Ober-Blöbaum, and K. Padberg-Gehle, Springer International Publishing, Cham, 2020, pp. 295–311.
- [43] Sarkka, S., and Sottinen, T., “Application of Girsanov Theorem to Particle Filtering of Discretely Observed Continuous-Time Non-Linear Systems,” *Bayesian Analysis*, Vol. 3, No. 3, 2008, pp. 555–584.
- [44] Grossman, R. L., Nerode, A., Ravn, A. P., and Rischel, H., *Hybrid Systems*, Vol. 736, Springer, 1993.
- [45] Posa, M., Cantu, C., and Tedrake, R., “A Direct Method for Trajectory Optimization of Rigid Bodies Through Contact,” *The International Journal of Robotics Research*, Vol. 33, No. 1, 2014, pp. 69–81.

- [46] Rijnen, M., Saccon, A., and Nijmeijer, H., “On optimal trajectory tracking for mechanical systems with unilateral constraints,” *IEEE Conference on Decision and Control (CDC)*, 2015, pp. 2561–2566.
- [47] Rijnen, M., Mooij, E. D., Traversaro, S., Nori, F., Wouw, N. V. D., Saccon, A., and Nijmeijer, H., “Control of humanoid robot motions with impacts: Numerical experiments with reference spreading control,” *IEEE International Conference on Robotics and Automation (ICRA)*, 2017, pp. 4102–4107.
- [48] Filippov, A. F., *Differential Equations with Discontinuous Righthand Sides: Control Systems*, Mathematics and its Applications, Vol. 18, Springer Science & Business Media, 2013. <https://doi.org/10.1007/978-94-015-7793-9>.
- [49] Muñoz, J.-G., Pérez, A., and Angulo, F., “Enhancing the Stability of the Switched Systems Using the Saltation Matrix,” *International Journal of Structural Stability and Dynamics*, Vol. 19, No. 05, 2019, p. 1941004. <https://doi.org/10.1142/S0219455419410049>.
- [50] Bai, S., Pan, Q., Ding, R., Jia, H., Yang, Z., and Chirarattananon, P., “An agile monopedal hopping quadcopter with synergistic hybrid locomotion,” *Science Robotics*, Vol. 9, 2024. URL <https://api.semanticscholar.org/CorpusID:269033494>.
- [51] Varsi, A., Taylor, J., Kekempanos, L., Pyzer Knapp, E., and Maskell, S., “A Fast Parallel Particle Filter for Shared Memory Systems,” *IEEE Signal Processing Letters*, Vol. 27, 2020, pp. 1570–1574. <https://doi.org/10.1109/LSP.2020.3014035>.
- [52] Nicely, M. A., and Wells, B. E., “Improved Parallel Resampling Methods for Particle Filtering,” *IEEE Access*, Vol. 7, 2019, pp. 47593–47604. <https://doi.org/10.1109/ACCESS.2019.2910163>.
- [53] Kim, J.-H., Hong, S., Ji, G., Jeon, S., Hwangbo, J., Oh, J.-H., and Park, H.-W., “Legged Robot State Estimation With Dynamic Contact Event Information,” *IEEE Robotics and Automation Letters*, Vol. 6, No. 4, 2021, pp. 6733–6740. <https://doi.org/10.1109/LRA.2021.3093876>.
- [54] Li, S., Lyu, S., and Trinkle, J., “State estimation for dynamic systems with intermittent contact,” *2015 IEEE International Conference on Robotics and Automation (ICRA)*, 2015, pp. 3709–3715. <https://doi.org/10.1109/ICRA.2015.7139714>.
- [55] Agogino, A. K., SunSpiral, V., and Atkinson, D., “Super Ball Bot - Structures for Planetary Landing and Exploration,” Technical Report HQ-E-DAA-TN63111, National Aeronautics and Space Administration, NASA Ames Research Center, Moffett Field, CA, USA, November 2018. URL <https://ntrs.nasa.gov/citations/20190001164>, nASA Technical Reports Server Document ID 20190001164.